# Synthesis strategies toward improved ordering of [$MnO_6$] octahedra in tunnel structured 2×3 and 2×4 $MnO_2$

Ryan Andris[a], Phillip Ridley[a], Bryan W. Byles[a], David A. Cullen[b], Karren L. More[b], and Ekaterina Pomerantseva[a*]

[a] Department of Materials Science and Engineering, Drexel University, Philadelphia, PA 19104, USA

[b] Center for Nanophase Materials Sciences, Oak Ridge National Laboratory, Oak Ridge, TN 37831, USA

* Corresponding author: ep423@drexel.edu

**Keywords:** manganese oxides, tunnel crystal structures, nanowires, control of the tunnel size, synthesis parameters

## ABSTRACT

Improved homogeneity of tunnel size in Na-stabilized 2×3 and 2×4 $MnO_2$ structures was achieved by identifying and controlling critical synthesis parameters. 2×3 and 2×4 $MnO_2$ tunnel manganese oxide nanowires were obtained by hydrothermal treatment of Na-birnessite, a layered manganese oxide that undergoes a layer-to-tunnel transition under high pressure and temperature. Herein, the improved ordering of [$MnO_6$] octahedra is revealed via a combined analysis of X-ray diffraction patterns and scanning transmission electron microscopy images. We show that crystallinity of the Na-birnessite precursor and the chemical composition of the system during hydrothermal treatment are crucial for achieving the targeted size of the structural tunnels with adequate uniformity.

## INTRODUCTION

Manganese oxides are considered an ideal platform for the development of next-generation energy storage solutions, hybrid capacitive water desalination approaches, and electrocatalysts owing to their low cost, low toxicity and high redox activity [1-6]. The structure of tunnel manganese oxides (TuMOs) is constructed from corner- and edge-sharing [$MnO_6$] octahedra units. These units form one-dimensional (1D) channels (or tunnels) with free volume available for ion intercalation [7-9]. There are several TuMO polymorphs with tunable tunnel size, which can be achieved by carefully controlling the synthesis parameters and the nature of the templating or stabilizing ions partially occupying the tunnel space. The tunnel polymorphs are typically distinguished by counting the number of [$MnO_6$] octahedra in the vertical and horizontal tunnel walls (e.g. 2×2, 2×3, 2×4 or 3×3 $MnO_2$). Therefore, these materials provide an excellent model system to investigate the relationships between tunnel size and ion size in applications that involve the reversible intercalation of ions from electrolytes or solutions. However, synthesis of TuMOs with uniform tunnel size is challenging, especially as the tunnel size increases [10-12].

Synthesis protocols for TuMOs with different tunnel sizes and stabilizing ions were extensively developed in the 1990s-2000s [7-9]. However, due to limited characterization capabilities, the structure of most of the synthesized materials was determined using bulk diffraction measurements that are unable to reveal local structural features. The most commonly used synthesis method for TuMOs with large tunnel sizes is hydrothermal treatment of layered manganese oxide precursors [7-9]. This approach often yields high aspect ratio 1D nanostructures, such as nanowires, with the structural tunnels running along the nanowire length. Therefore, TuMO nanowires established themselves as ideal model materials to study nanoscale mechanical properties [13-15] ion diffusion using *in situ* transmission electron microscopy (TEM) and structural evolution during electrochemical cycling [11, 16-22]. TEM investigations have also revealed tunnel size heterogeneity in manganese oxide with todorokite crystal structure (3 x 3 $MnO_2$) [10, 12]. However, little is known about TuMOs with large tunnel sizes other than todorokite-$MnO_2$.

2×3 and 2×4 $MnO_2$ are characterized by 7.2 Å x 9.6 Å and 7.2 Å x 12.6 Å rectangular tunnels, respectively, with distances measured between the corresponding Mn atoms in the tunnel walls (**Figure S1** in Supporting Information) [23-25]. In both materials, the tunnel space is partially occupied by $Na^+$ ions, making them particularly promising for use as electrodes in Na-ion batteries and hybrid capacitive deionization devices for removal of NaCl from water. Indeed, it was previously shown that these diffusion processes can be facilitated when intercalation sites in the host electrode material are well-defined through chemical pre-intercalation of ions of the same nature as electrochemically cycled ions, leading to improved performance [26].

2×4 $MnO_2$ is usually prepared through hydrothermal treatment of the layered Na-birnessite powder in the presence of excess sodium ions sourced from either NaCl or NaOH solution [24, 27-30].

Cetyltrimethylammonium bromide (CTAB) assisted synthesis was also reported [31, 32]. Fewer reports on the synthesis of 2×3 $MnO_2$ exist [23, 33-35], and some of the published findings focus on Ba- and Li-exchanged phases [34, 35]. The hydrothermal treatment conditions for the preparation of 2×3 $MnO_2$ TuMO are believed to require only deionized water in the absence of any additional Na source except for the ions residing in the interlayer region of Na-birnessite precursor [23]. Still, the synthesis conditions vary between each report, and in many cases, only brief descriptions are given without detailed discussion of the parameters. Moreover, the characterization of the produced TuMOs is often limited to X-ray diffraction, which only provides information about bulk average material structure. As shown previously for todorokite $MnO_2$, the radial nanowire scanning transmission electron microscopy (STEM) images can be misleading by showing only one dimension of the tunnel [36], while cross-sectional STEM imaging of the same samples clearly demonstrates tunnel size inhomogeneity [10, 11, 37]. Therefore, without local structure characterization, it is impossible to reliably develop synthesis approaches for the preparation of TuMO phases with the uniform tunnel size. These methods are required in order to understand the fundamental structure-property relationships of TuMOs.

In this work, we for the first time show cross-sectional STEM images of 2×3 and 2×4 $MnO_2$ nanowires clearly demonstrating improved ordering of [$MnO_6$] octahedra leading toward more uniform tunnel size. Through the detailed synthesis and STEM analysis we established that the homogeneity of tunnel sizes can be achieved through improved crystallinity of the layered Na-birnessite precursor material via extended aging and delicate control over the pH of the solutions during washing and hydrothermal treatment. A high degree of tunnel size homogeneity opens opportunities for establishing relationships between tunnel size and electrochemically cycled ions. In turn, we can provide insights into the design and synthesis of intercalation hosts for electrochemically-driven applications. The knowledge gained from studying TuMOs can be extended to other intercalation compounds and enable new solutions for a sustainable future.

## EXPERIMENTAL METHODS

2×3 and 2×4 $MnO_2$ nanowires, stabilized with sodium ions and water molecules ($Na_xMnO_2{\cdot}nH_2O$), were synthesized via hydrothermal treatment of the layered Na-birnessite precursor, following previously reported procedures [23-25]. The Na-birnessite precursor was prepared via dropwise addition of a chilled 50 mL solution of 0.3 M $Mn(Cl)_2{\cdot}4H_2O$ (Acros Organics) to a 50 mL solution of 3.0 M NaOH (Fisher Scientific) and 0.79 g of $KMnO_4$ (Acros Organics) in an ice bath over a 15 minute time period. After a dark brown precipitate formed, the mixture was removed from the ice bath, statically aged for one week, then washed with deionized water and filtered until the filtrate reached a pH of approximately 7. The filtrate was dried at 105 °C in air overnight.

2×3 $MnO_2$ nanowires were prepared by adding 100 mg of dry Na-birnessite powder to 11.5 mL of DI water in a 23 mL Teflon-line stainless steel autoclave (Parr Instruments) and hydrothermally treated at 220 ºC for 96 h. 2×4 $MnO_2$ nanowires were synthesized by adding 500 mg of dry Na-birnessite powder to 11.5 mL of 1 M NaOH solution (Fischer Scientific) in a 23 mL Teflon-lined stainless steel autoclave, and hydrothermally treated at 220 ºC for 96 h. The resultant nanowires were filtered, washed with deionized water until neutral pH of the filtrate was achieved. For comparison, 2×n $MnO_2$ and hybrid-$MnO_2$ nanowires were synthesized following the previously reported procedures [37]. 2×n $MnO_2$ phase was obtained by aging Na-birnessite for four days. The resulting powder was filtered, washed, and dried at 100 °C for 12 h. 100 mg of dry Na-birnessite was added to 15 mL of deionized water in a 23 mL Teflon-lined stainless steel autoclave and placed in an oven at 220°C for 192 h. The highly disordered hybrid-$MnO_2$ phase was obtained by aging Na-birnessite for only 1 h followed by hydrothermal treatment under the same conditions. After hydrothermal treatment, all products were filtered, washed, and dried at 100 °C for 12 h. The synthesis schematic shown in **Figure 1** highlights the parameters that we found to be important for achieving tunnel size homogeneity.

The XRD patterns of the synthesized materials were obtained using a Rigaku benchtop powder X-ray diffractometer with $Cu_{k\alpha}$ ($\lambda$ =1.54 Å) radiation with 0.02° step size, and step speed of 0.6 °/min. Morphology of the particles was investigated using a Zeiss Supra 50VP scanning electron microscope (SEM) equipped with a Schottky field emission gun and Everhart-Thornley in-lens secondary electron detector. Images were acquired using a beam accelerating voltage between 3-5 kV, and working distances between 4-7 mm. Additionally, samples were sputter coated with a thin 5-10 nm layer of Pt/Pd to prevent charging and improve image quality.

Manganese oxide nanowires were embedded in epoxy and cross-sectioned by diamond-knife ultramicrotomy in preparation for analysis by aberration-corrected STEM. High-angle annular dark field (HAADF) images were acquired using a JEOL JEM 2200FS TEM/STEM operated at 200 kV and equipped with a CEOS probe Cs-corrector.

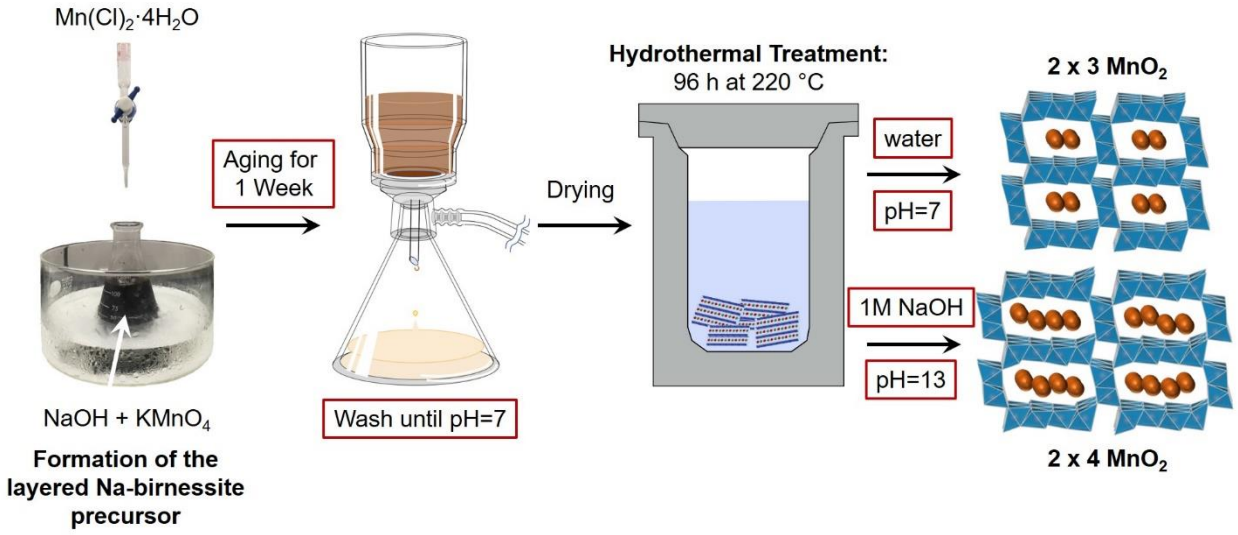


**Figure 1.** Schematic illustration showing the synthesis process for the preparation of 2×3 $MnO_2$ and 2×4 $MnO_2$ nanowires with tunnel structures. The parameters found in this work to be critical for improving tunnel size homogeneity are outlined in red.

## RESULTS AND DISCUSSION

SEM images of the synthesized tunnel manganese oxides demonstrate 1D morphology (**Figure 2**), in agreement with previous reports [23-25, 37]. We have not thoroughly analyzed the cross-sections of the obtained 1D nanostructures; therefore, in this paper we will call them nanowires based on diameter-to-length ratio. The nanowires form porous networks of flexible 1D nanoparticles. The hybrid-$MnO_2$ nanowires (**Figure 1a**) are 10 – 50 nm in diameter and up to several microns long. **Figure 2b** shows that the 2×n $MnO_2$ nanowires are similar in length, but their diameters are as large as 250 nm. The nanowires of 2×3 $MnO_2$ material exhibit diameters in the range of 25 - 75 nm and lengths up to ~100 μm (**Figure 2c**). Similarly, the 2×4 $MnO_2$ nanoparticles display the diameters of 10 – 100 nm and lengths up to several tens of micrometers. However, the 2×4 $MnO_2$ nanowires appear to be more densely packed compared to 2×3 $MnO_2$ analogs (**Figure 2d**).

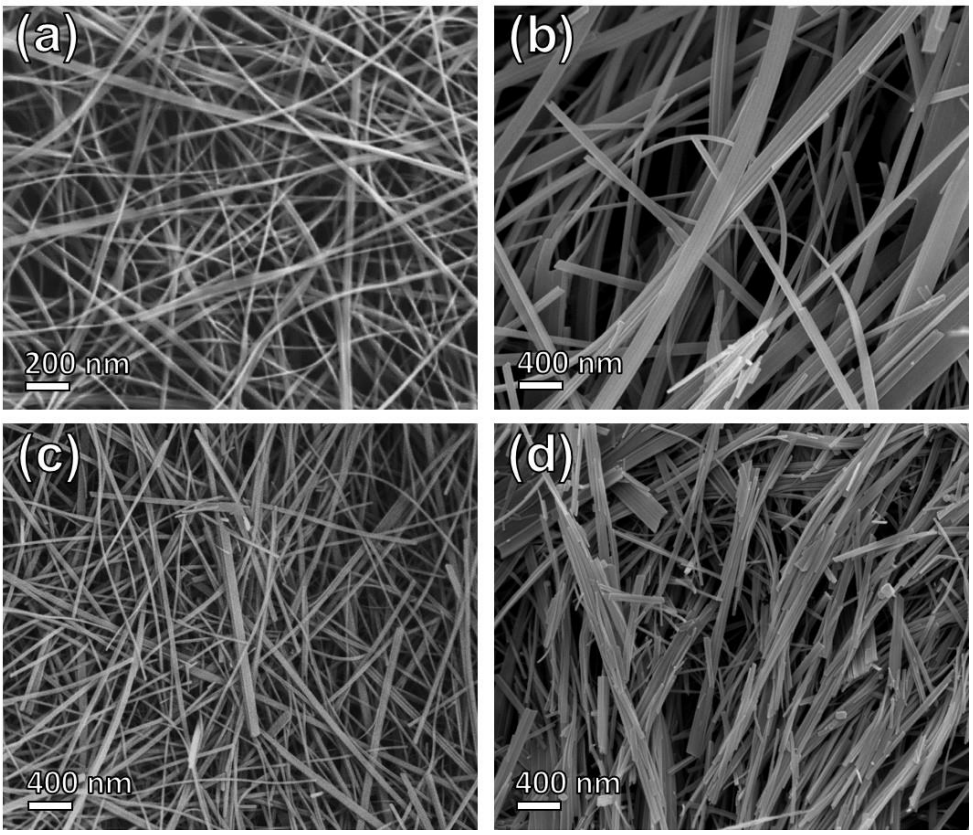


**Figure 2.** SEM images of (a) hybrid-$MnO_2$, (b) 2×n-$MnO_2$, (c) 2×3-$MnO_2$ and (d) 2×4-$MnO_2$ nanowires.

**Figure 3a** shows how the XRD patterns of the nanowires collected as the aging time of the Na-birnessite precursor increased from 1 h to 1 week and the pH of solutions at different stages of the synthesis was more thoroughly controlled. The Na-birnessite was aged for only 1 hour to obtain hybrid-$MnO_2$ nanowires. The corresponding XRD pattern shows few distinguishable, broad reflections with large full-width at half-maximum (FWHM), indicating a highly disordered phase with small crystallite sizes. This result is in good agreement with the cross-sectional HAADF-STEM image (**Figure 4a**) demonstrating highly aperiodic and disordered tunnel dimensions. There are tunnel sizes ranging from 2×2 to 2×5 among regions that appear to be amorphous, all within the single nanowire. The Na-birnessite aging time was increased from 1 hour to 4 days to produce 2×n $MnO_2$ material. The XRD pattern of the hydrothermally treated product exhibited more reflections with smaller FWHMs compared to that of hybrid-$MnO_2$ indicating improved crystallinity of the material (**Figure 3a**). Increasing the aging time further to one week, combined with thorough washing of the filtrate to achieve a pH of ~7, resulted in the appearance of new Bragg peaks in the XRD pattern of the hydrothermally treated product (**Figure 3a**). In fact, the XRD pattern of this material is in excellent agreement with the previously reported XRD pattern of 2×3 $MnO_2$ phase [25].

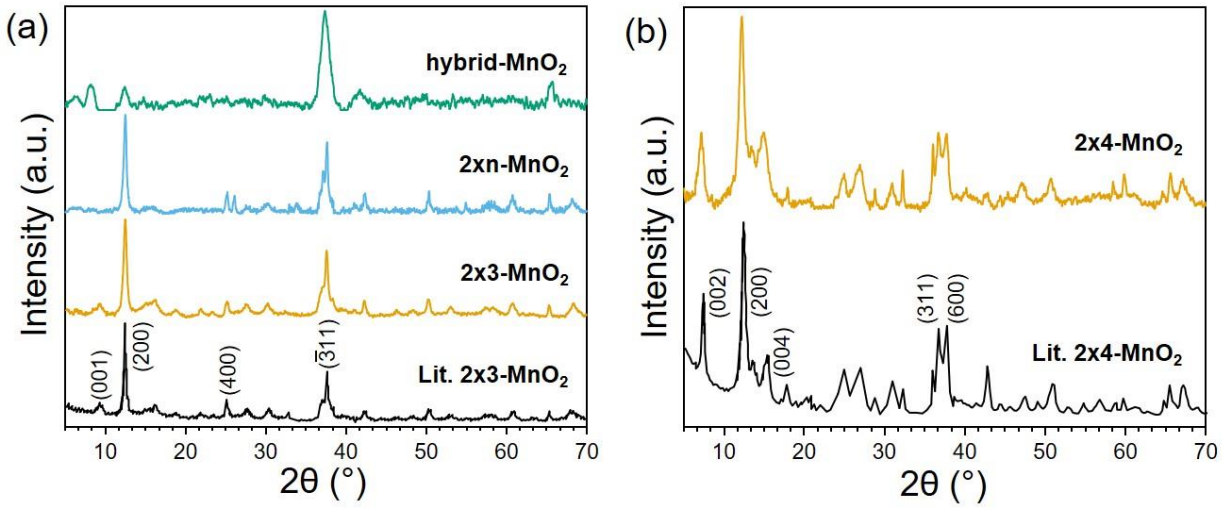


**Figure 3.** XRD patterns showing (a) the progression of 2×3-$MnO_2$ nanowires synthesis and (b) 2×4-$MnO_2$ nanowires prepared using synthesis parameters revealed during synthesis of 2×3-$MnO_2$ nanowires. The literature patterns are from [25].

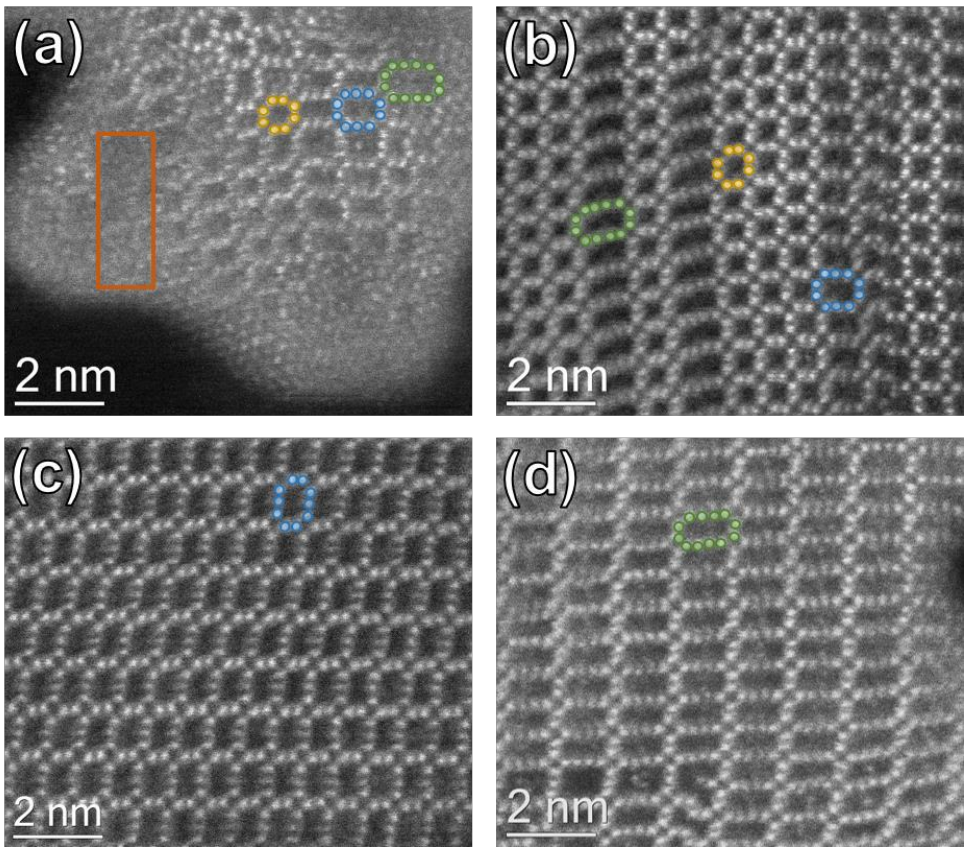


**Figure 4.** Cross-sectional HAADF-STEM images of (a) hybrid-$MnO_2$, (b) 2×n-$MnO_2$, (c) 2×3-$MnO_2$ and (d) 2×4-$MnO_2$ nanowires. The colored circles, each representing an $MnO_6$ octahedra, denote different tunnel sizes: yellow – 2×2 tunnels, blue – 2×3 tunnels, green – 2×4 tunnels. The orange box in (a) is a region with incompletely formed tunnels.

The cross-sectional HAADF-STEM image of 2×n $MnO_2$ nanowire (**Figure 4b**) reveals the presence of 2×2, 2×3 and 2×4 tunnels within a single nanowire. The common 2 [$MnO_6$] octahedra dimension corresponds to the (200) lattice plane ($d$ ~6.98 Å) which is in agreement with reflections in the XRD pattern of this material ($d$ ~7.1 Å) (**Figure 3a**). In addition, the variable size of the perpendicular tunnel wall introduces disorder reflected by the absence of certain reflections in the XRD data. Most prominently, the XRD pattern of the 2×n $MnO_2$ does not have the (001) peak at 9.2° 2θ that corresponds to a tunnel side of 3 [$MnO_6$] octahedra (~9.6 Å). The absence of this peak indicates that 2×n $MnO_2$ nanowires do not have an ordered occurrence of the tunnel wall of this size, in agreement with the cross-sectional HAADF-STEM imaging. In contrast, the (001) peak at 9.2° 2θ in the 2×3 $MnO_2$ material XRD pattern (**Figure 3a**) indicates the regular formation of tunnel walls built by 3 [$MnO_6$] octahedra. The regular array of 2×3 tunnels is clearly observed in the cross-sectional HAADF-STEM image of the 2×3 $MnO_2$ nanowire shown in **Figure 4c**. The improved tunnel size homogeneity was achieved by extended aging of Na-birnessite precursor and thorough washing prior to hydrothermal treatment. Extended aging time could lead to the $Mn^{3+}/Mn^{4+}$ ordering in birnessite layers, which was previously found to have a significant effect on the layer-to-tunnel transition kinetics [10]. Moreover, the system used for Na-birnessite synthesis requires large amounts of water to neutralize unreacted NaOH in the filtrate. If NaOH is not fully washed, it will be transferred into the hydrothermal treatment container, leading to conditions resembling those used for the synthesis of 2×4 $MnO_2$ nanowires. This hypothesis is supported by cross-sectional HAADF-STEM characterization clearly showing formation of the 2×4 tunnels in the structure of 2×n $MnO_2$ nanowires (**Figure 4b**).

Successful preparation of the 2×3 $MnO_2$ nanowires revealed important parameters that could also be controlled during the synthesis of 2×4 $MnO_2$ phase. The 2×4 $MnO_2$ XRD pattern is shown in **Figure 3b,** and it is in excellent agreement with the literature [23]. The characteristic diffraction peaks for 2×4 tunnels are found at $d$ ~7.2 Å and $d$ ~12.2 Å respectively (i.e. (200) and (002) planes). Cross-sectional HAADF-STEM imaging confirms the presence of a large fraction of 2×4 tunnels (**Figure 4d**). However, a single 2×4 $MnO_2$ nanowire exhibits a greater degree of tunnel size inhomogeneity than 2×3 $MnO_2$ phase. There is evidence for the presence of of 3×4 and 2×5 tunnels (**Figure 4d**). More corroboration of the slight disparity in structural order is shown in additional cross-sectional HAADF-STEM images (**Figure S2** in Supporting Information). The 2×4 tunnels are larger than 2×3 tunnels and therefore the higher degree of [$MnO_6$] octahedra disorder is in agreement with the investigations of manganese dioxide with todorokite (3×3) structure [10-12]. Further improvements in the synthesis of 2×4 $MnO_2$ phase with homogeneous tunnel size could be achieved by increasing sodium concentration in solution during hydrothermal treatment step [24].

## CONCLUSIONS

We demonstrate the synthesis of 2×3 $MnO_2$ and 2×4 $MnO_2$ nanowires with improved tunnel size uniformity. The structure and tunnel size homogeneity are confirmed via a combination of XRD and cross-sectional STEM imaging. Improved ordering of [$MnO_6$] octahedra was achieved by statically aging the layered Na-birnessite precursor for one week, leading to increased crystallinity. We also found that the pH of the solution during hydrothermal treatment is critical for controlling the size and uniformity of the structural tunnels. The $Na^+$ ions that stabilize the tunnels have increased radii in basic solutions that result in increased tunnel dimensions. Therefore, the Na-birnessite precursor needs to be thoroughly washed and the pH of the filtrate solution needs to be well controlled prior to hydrothermal treatment. Our findings are crucial for the establishment of accurate structure-property relationships for tunnel manganese oxides.


## ACKNOWLEDGEMENTS

E. Pomerantseva acknowledges funding from the National Science Foundation (Grants CMMI-1635233 and CBET-1604483). We thank Drexel's Centralized Research Facilities for help with materials characterization. STEM imaging was conducted at the Center for Nanophase Materials Sciences, which is a DOE Office of Science User Facility.


## AUTHOR INFORMATION:


Corresponding Author

Email: ep423@drexel.edu


Author Contributions

E.P. developed the concept and designed the experiments. R.A., P.R. and B.B. carried out experimental work. D.C. and K.M. performed STEM analysis. All authors contributed to the analysis and interpretation of the obtained experimental data and writing of this manuscript.

**REFERENCES**


1. Kuo, C.H., I.M. Mosa, A.S. Poyraz, S. Biswas, A.M. E-Sawy, W.Q. Song, Z. Luo, S.Y. Chen, J.F. Rusling, J. He, and S.L. Suib, *Robust Mesoporous Manganese Oxide Catalysts for Water Oxidation.* Acs Catalysis, 2015. **5**(3): p. 1693-1699.
2. Lee, J., S. Kim, C. Kim, and J. Yoon, *Hybrid capacitive deionization to enhance the desalination performance of capacitive techniques.* Energy & Environmental Science, 2014. **7**(11): p. 3683-3689.
3. Ortiz-Vitoriano, N., N.E. Drewett, E. Gonzalo, and T. Rojo, *High performance manganese-based layered oxide cathodes: overcoming the challenges of sodium ion batteries.* Energy & Environmental Science, 2017. **10**(5): p. 1051-1074.
4. Stoerzinger, K.A., M. Risch, B.H. Han, and Y. Shao-Horn, *Recent Insights into Manganese Oxides in Catalyzing Oxygen Reduction Kinetics.* ACS Catalysis, 2015. **5**(10): p. 6021-6031.
5. Thackeray, M.M., C.S. Johnson, J.T. Vaughey, N. Li, and S.A. Hackney, *Advances in manganese-oxide 'composite' electrodes for lithium-ion batteries.* Journal of Materials Chemistry, 2005. **15**(23): p. 2257-2267.
6. Wei, W.F., X.W. Cui, W.X. Chen, and D.G. Ivey, *Manganese oxide-based materials as electrochemical supercapacitor electrodes.* Chemical Society Reviews, 2011. **40**(3): p. 1697-1721.
7. Brock, S.L., N.G. Duan, Z.R. Tian, O. Giraldo, H. Zhou, and S.L. Suib, *A review of porous manganese oxide materials.* Chemistry of Materials, 1998. **10**(10): p. 2619-2628.
8. Feng, Q., H. Kanoh, and K. Ooi, *Manganese oxide porous crystals.* Journal of Materials Chemistry, 1999. **9**(2): p. 319-333.
9. Suib, S.L., *Porous manganese oxide octahedral molecular sieves and octahedral layered materials.* Accounts of Chemical Research, 2008. **41**(4): p. 479-487.
10. Yuan, Y., K. He, B.W. Byles, C. Liu, K. Amine, J. Lu, E. Pomerantseva, and R. Shahbazian-Yassar, *Deciphering the Atomic Patterns Leading to $MnO_2$ Polymorphism.* Chem, 2019. **5**(7): p. 1793-1805.
11. Yuan, Y., C. Liu, B.W. Byles, W. Yao, B. Song, M. Cheng, Z. Huang, K. Amine, E. Pomerantseva, R. Shahbazian-Yassar, and J. Lu, *Ordering Heterogeneity of [MnO6] Octahedra in Tunnel-Structured $MnO_2$ and Its Influence on Ion Storage.* Joule, 2019. **3**(2): p. 471-484.
12. Hu, X.B., D.A. Kitchaev, L.J. Wu, B.J. Zhang, Q.P. Meng, A.S. Poyraz, A.C. Marschilok, E.S. Takeuchi, K.J. Takeuchi, G. Ceder, and Y.M. Zhu, *Revealing and Rationalizing the Rich Polytypism of Todorokite $MnO_2$.* Journal of the American Chemical Society, 2018. **140**(22): p. 6961-6968.
13. Maksud, M., M. Barua, M.R.A. Shikder, B.W. Byles, E. Pomerantseva, and A. Subramanian, *Tunable nanomechanical performance regimes in ceramic nanowires.* Nanotechnology, 2019. **30**(47): p. 47LT02.
14. Amin Shikder, M.R., M. Maksud, G. Vasudevamurthy, Bryan W. Byles, D.A. Cullen, K.L. More, E. Pomerantseva, and A. Subramanian, *Brittle fracture to recoverable plasticity: polytypism-dependent nanomechanics in todorokite-like nanobelts.* Nanoscale Advances, 2019. **1**(1): p. 357-366.
15. Maksud, M., N.K.R. Palapati, B.W. Byles, E. Pomerantseva, Y. Liu, and A. Subramanian, *Dependence of Young's modulus on the sodium content within the structural tunnels of a one-dimensional Na-ion battery cathode.* Nanoscale, 2015. **7**(42): p. 17642-17648.
16. Housel, L.M., L. Wang, A. Abraham, J.P. Huang, G.D. Renderos, C.D. Quilty, A.B. Brady, A.C. Marschilok, K.J. Takeuchi, and E.S. Takeuchi, *Investigation of a-$MnO_2$ Tunneled Structures as Model Cation Hosts for Energy Storage.* Accounts of Chemical Research, 2018. **51**(3): p. 575-582.
17. Lee, S.Y., L.M. Housel, J.P. Huang, L.J. Wu, E.S. Takeuchi, A.C. Marschilok, K.J. Takeuchi, M. Kim, and Y.M. Zhu, *Inhomogeneous structural evolution of silver-containing a-$MnO_2$ nanorods in sodium-ion batteries investigated by comparative transmission electron microscopy approach.* Journal of Power Sources, 2019. **435**.

18. Lee, S.Y., L.J. Wu, A.S. Poyraz, J.P. Huang, A.C. Marschilok, K.J. Takeuchi, E.S. Takeuchi, M. Kim, and Y.M. Zhu, *Lithiation Mechanism of Tunnel-Structured $MnO_2$ Electrode Investigated by In Situ Transmission Electron Microscopy.* Advanced Materials, 2017. **29**(43).
19. Yang, S.Z., K.R. Tallman, P. Liu, D.M. Lutz, B.J. Zhang, S.J. Kim, L.J. Wu, A.C. Marschilok, E.S. Takeuchi, K.J. Takeuchi, and Y.M. Zhu, *The effects of vanadium substitution on one-dimensional tunnel structures of cryptomelane: Combined TEM and DFT study.* Nano Energy, 2020. **71**.
20. Yuan, Y.F., A.M. Nie, G.M. Odegard, R. Xu, D.H. Zhou, S. Santhanagopalan, K. He, H. Asayesh-Ardakani, D.D. Meng, R.F. Klie, C. Johnson, J. Lu, and R. Shahbazian-Yassar, *Asynchronous Crystal Cell Expansion during Lithiation of $K^+$-Stabilized a-$MnO_2$.* Nano Letters, 2015. **15**(5): p. 2998-3007.
21. Yuan, Y.F., S.M. Wood, K. He, W.T. Yao, D. Tompseett, J. Lu, A.M. Nie, M.S. Islam, and R. Shahbazian-Yassar, *Atomistic Insights into the Oriented Attachment of Tunnel-Based Oxide Nanostructures.* ACS Nano, 2016. **10**(1): p. 539-548.
22. Yuan, Y.F., C. Zhan, K. He, H.R. Chen, W.T. Yao, S. Sharifi-Asl, B. Song, Z.Z. Yang, A.M. Nie, X.Y. Luo, H. Wang, S.M. Wood, K. Amine, M.S. Islam, J. Lu, and R. Shahbazian-Yassar, *The influence of large cations on the electrochemical properties of tunnel-structured metal oxides.* Nature Communications, 2016. **7**.
23. Shen, X.F., Y.S. Ding, J. Liu, K. Laubernds, R.P. Zerger, M. Polverejan, Y.C. Son, M. Aindow, and S.L. Suib, *Synthesis, characterization, and catalytic applications of manganese oxide octahedral molecular sieve (OMS) nanowires with a 2 x 3 tunnel structure.* Chemistry of Materials, 2004. **16**(25): p. 5327-5335.
24. Xia, G.G., W. Tong, E.N. Tolentino, N.G. Duan, S.L. Brock, J.Y. Wang, S.L. Suib, and T. Ressler, *Synthesis and characterization of nanofibrous sodium manganese oxide with a 2 x 4 tunnel structure.* Chemistry of Materials, 2001. **13**(5): p. 1585-1592.
25. Shen, X.F., Y.S. Ding, J. Liu, J. Cai, K. Laubernds, R.P. Zerger, A. Vasiliev, M. Aindow, and S.L. Suib, *Control of nanometer-scale tunnel sizes of porous manganese oxide octahedral molecular sieve nanomaterials.* Advanced Materials, 2005. **17**(7): p. 805-+.
26. Clites, M., J.L. Hart, M.L. Taheri, and E. Pomerantseva, *Chemically Preintercalated Bilayered $K_xV_2O_5{\cdot}nH_2O$ Nanobelts as a High-Performing Cathode Material for K-Ion Batteries.* ACS Energy Letters, 2018. **3**(3): p. 562-567.
27. Feng, Q., *Synthesis of Cs-birnessite and transformation reaction to (2 x 4) tunnel structure by heat-treatment.* Journal of Materials Science Letters, 2003. **22**(14): p. 999-1001.
28. Liu, Z.H. and K. Ooi, *Preparation and alkali-metal ion extraction/insertion reactions with nanofibrous manganese oxide having 2 x 4 tunnel structure.* Chemistry of Materials, 2003. **15**(19): p. 3696-3703.
29. Rasul, S., S. Suzuki, S. Yamaguchi, and M. Miyayama, *Manganese oxide octahedral molecular sieves as insertion electrodes for rechargeable Mg batteries.* Electrochimica Acta, 2013. **110**: p. 247-252.
30. Poyraz, A.S., C.D. Quilty, L.M. Housel, X.B. Hu, A.M. Bruck, Y.R. Li, J.F. Yin, B.J. Zhang, J.P. Huang, L.J. Wu, Y.M. Zhu, E.S. Takeuchi, A.C. Marschilok, and K.J. Takeuchi, *Synthesis and Characterization of 2 x 4 Tunnel Structured Manganese Dioxides as Cathodes in Rechargeable Li, Na, and Mg Batteries.* Journal of the Electrochemical Society, 2019. **166**(4): p. A670-A678.
31. Kuratani, K., K. Tatsumi, and N. Kuriyama, *Manganese oxide nanorod with 2 x 4 tunnel structure: Synthesis and electrochemical properties.* Crystal Growth & Design, 2007. **7**(8): p. 1375-1377.
32. Kuratani, K., K. Tatsumi, and N. Kuriyama, *Synthesis and Electrochemical Performance of Manganese Oxide.* ECS Transactions, 2019. **6**(25): p. 279-286.
33. Li, J.Y., X.L. Wu, X.H. Zhang, H.Y. Lu, G. Wang, J.Z. Guo, F. Wan, and R.S. Wang, *Romanechite-structured $Na_{0.31}MnO_{1.9}$ nanofibers as high-performance cathode material for a sodium-ion battery.* Chemical Communications, 2015. **51**(80): p. 14848-14851.
34. Tsuda, M., H. Arai, Y. Nemoto, and Y. Sakurai, *Electrode performance of romanechite for rechargeable lithium batteries.* Journal of Power Sources, 2001. **102**(1-2): p. 135-138.

35. Tsuda, M., H. Arai, Y. Nemoto, and Y. Sakurai, *Electrode performance of sodium and lithium-type romanechite.* Journal of the Electrochemical Society, 2003. **150**(6): p. A659-A664.
36. Byles, B.W., P. West, D.A. Cullen, K.L. More, and E. Pomerantseva, *Todorokite-type manganese oxide nanowires as an intercalation cathode for Li-ion and Na-ion batteries.* RSC Advances, 2015. **5**(128): p. 106265-106271.
37. Byles, B.W., D.A. Cullen, K.L. More, and E. Pomerantseva, *Tunnel structured manganese oxide nanowires as redox active electrodes for hybrid capacitive deionization.* Nano Energy, 2018. **44**: p. 476-488.